Available online at www.sciencedirect.com
SCIENCE DIRECT
Journal of Power Sources 155 (2006) 478–486
JOURNAL OF POWER SOURCES
www.elsevier.com/locate/jpowsour

Power conditioning for a wind–hydrogen energy system

Hernán De Battista[a]*, Ricardo Julián Mantz[b], Fabricio Garelli[a]

[a] CONICET, LEICI, Faculty of Engineering, National University of La Plata, C.C.91 (1900) La Plata, Argentina
[b] CICpBA, LEICI, Faculty of Engineering, National University of La Plata, C.C.91 (1900) La Plata, Argentina

Received 11 April 2005; received in revised form 10 May 2005; accepted 11 May 2005
Available online 22 June 2005

Abstract

In addition to the efforts to reduce the costs of renewable energy technologies and electrolyzers, the development of suitable controllers are needed for cost-competitive electricity production by renewable-hydrogen power plants. In this paper, a novel control is proposed for a wind-electrolysis system, which match the wind power output to the electrolyzer power requirements, thus gaining in system performance. It basically consists in continuously shaping the power reference of a conventional maximum power point tracking algorithm. Thus, high aerodynamic power conversion efficiency is achieved fulfilling at the same time the electrolyzer specifications. This control strategy is developed using concepts of the reference conditioning technique and of the sliding mode control theory. The proposed control algorithm is extremely simple, easy to implement and robust to parameter uncertainties.

Keywords: Electrolysis; Hydrogen; Wind energy; Sliding mode control; Power limiting

1. Introduction

Clean and sustainable electricity generation from renewable resources have experienced a significant development during the last decades. Nowadays, alternative energy conversion systems are commonly found in different autonomous and grid-connected applications. However, the intermittent and seasonal variability of the primary resources hampers a greater penetration of these clean energies into the power generation market. The aggregation of different types of energy resources, for instance wind and solar, helps to attenuate this limitation. Nevertheless, the best solution consists in storing the energy captured in excess to be used during short-supply periods. Although batteries are extensively used in low power systems, their use in medium and large power applications is inviable because of their relatively low storage density (energy/volume). A feasible option is the production of hydrogen through water electrolysis for its subsequent use either to produce electricity or to supply fuel engines. In fact, hydrogen allows both storage and transportation of large amounts of energy at much higher energy densities [1–3]. Traditional storage options are actually viable for hydrogen consumption in large plants. Yet the on-board storage for use on light vehicles is an open problem being actively investigated [4].

Due to the comparatively low cost of wind technology, along with the persistent growth in installed wind power capacity over the world, wind-electrolysis is the favorite candidate to become the first economically viable renewable-hydrogen production system. Before this can be realized, however, optimization of the whole system is needed in addition to the ongoing efforts to reduce the costs of electrolysis technology. Many research projects and articles reported in the literature about hydrogen production plants are concerned with the sizing, economics and power flow management of the devices comprising the system (wind turbine, electrolyzer, batteries, etc.), in order to guarantee service quality at minimum cost. These problems are closely associated to the local resource characteristics [5–8].

Two different approaches are found with regards to the configuration of stand-alone wind-electrolysis system. In

* Corresponding author. Tel.: +54 221 4259306; fax: +54 221 4259306.
E-mail addresses: deba@ing.unlp.edu.ar (H. De Battista); mantz@ing.unlp.edu.ar (R.J. Mantz); fabricio@ing.unlp.edu.ar (F. Garelli).

0378-7753/$ – see front matter © 2005 Elsevier B.V. All rights reserved.
doi:10.1016/j.jpowsour.2005.05.005

most cases, the turbine and electrolyzer, with their own dedicated power electronics and controllers, are connected to a constant-voltage dc-bus. Such a decoupled configuration presents the advantage that the power converters of the turbine and the electrolyzer can be controlled separately. In this scheme, the variable-frequency variable-voltage ac at the wind-driven generator terminals is converted to the constant dc-bus voltage through an ac–dc converter, whereas a dc–dc converter takes the dc-bus voltage and provides a dc voltage suitable for electrolyzer operation. The voltage of this dc-bus is fixed by a battery pack, which also has to manage the power mismatches between the wind turbine and the electrolyzer and serves as a filter of the input power fluctuations.

A more recent approach proposes eliminating the component duplication in the interface between the turbine and the electrolyzer. In fact, the pair of power converters and the dc-bus can be replaced with a single ac–dc converter taking the ac generator voltage and providing an appropriate voltage to the electrolyzer. Thus, the efficiency of the energy conversion can be increased and the overall cost of the system can be appreciably reduced [9,10]. Obviously, this coupled configuration requires the development of controllers specifically designed for this application. In this context, the current paper addresses the control of a wind-powered hydrogen production system to match the input wind power to the electrolyzer requirements, thereby increasing the captured energy and improving the dynamic performance. Thus, the sizing of the system required to accomplish the specifications can be substantially reduced.

2. System description

2.1. The plant

The system under consideration is sketched in Fig. 1. Its main components are:

- *Wind turbine*. The dynamic behavior of the wind turbine can be described by the first-order differential equation:

$$\frac{d\Omega}{dt} = \frac{1}{J}(T_T - T_G) \tag{1}$$

where Ω is the shaft speed, J the inertia of the rotating parts, T_G the electric torque developed by the generator and T_T is the aerodynamic torque:

$$T_T(\lambda, w) = \frac{1}{2}\rho\pi r^3 C_T(\lambda) w^2. \tag{2}$$

This aerodynamic torque is a nonlinear function of the wind velocity w and the tip-speed-ratio $\lambda = r\Omega/w$, with r being the blades length and ρ being the air density. Fig. 2 displays the torque coefficient C_T (dashed line) as well as the power efficiency $C_P = \lambda C_T$ (solid line). Hence, the power captured by the turbine can be expressed as the product of this latter coefficient and the wind power [11]:

$$P_T(\lambda, w) = \frac{1}{2}\rho\pi r^2 C_P(\lambda) w^3. \tag{3}$$

As it can be observed in Fig. 2, the power conversion efficiency takes its maximum C_{Popt} at the optimum tip-speed-ratio λ_{opt}. So, fixed-speed wind turbines operate with maximum efficiency at just one wind velocity. Therefore, variable-speed controllers are commonly implemented in order to track the optimum power $P_{opt}(w) = P_T(\lambda_{opt}, w)$. This sort of control strategy is called maximum power point tracking (MPPT) controller.

- *Permanent magnet synchronous generator*. For the purposes of this work, the generator can be modeled as a three-phase sinusoidal voltage source E_F in series with a synchronous reactance X_S as shows the per-phase circuit sketched in Fig. 3. The phase current and voltage at the generator terminals are I_S and V_S, respectively. Note that the terminal voltage V_S slightly differs in magnitude and phase from the emf E_F because of the voltage drop across X_S when the current I_S passes through it. The mechanical variables of the generator, i.e. speed and torque, are related to the electrical ones as follows:

$$\begin{aligned} E_F &= \frac{p}{2}\Phi\Omega \\ T_G &= \frac{3 I_S V_S \cos\phi}{\Omega} \end{aligned} \tag{4}$$

where p is the number of poles of the machine, Φ the stator flux linkage and ϕ is the phase angle between V_S and I_S. The former equation is derived from electromagnetic considerations, whereas the latter is obtained from power balance between mechanical ($P_G = T_G\Omega$) and electrical ($P_S = 3 I_S V_S \cos\phi$) powers [12].

- *Electronic converter*. The electronic devices are aimed at converting the ac three-phase speed-dependent generator voltage V_S into a dc voltage V_H suitable for hydrogen production. As it was previously mentioned, a single ac–dc converter is considered in this paper as interface between the turbine and the electrolyzer. That is, the voltage at the generator terminals is directly converted to the voltage at the electrolyzer terminals. The output and input voltages of the converter are related by the controlled factor δ, which is associated to the duty cycle of the electronic switching devices. Since incoming and outgoing powers are matched, i.e. $P_S = P_H$, input and output currents have a similar ratio. That is,

$$\begin{aligned} \delta V_S &= V_H \\ \delta I_H &= 3 I_S \cos\phi. \end{aligned} \tag{5}$$

It is assumed in this paper that $\cos\phi = 1$, i.e. that the input voltage and current are in phase. This is the case in many ac–dc converters, such as those having an uncontrolled rectifier at the input [12].

- *Electrolyzer*. The electrolyzer is modeled by an empirically obtained current–voltage ($I_H - V_H$) curve. This

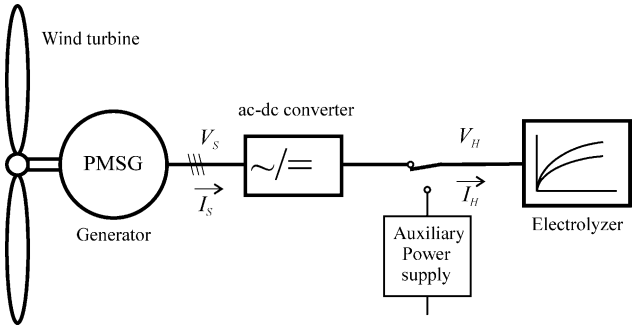

Fig. 1. Wind-powered hydrogen plant scheme.

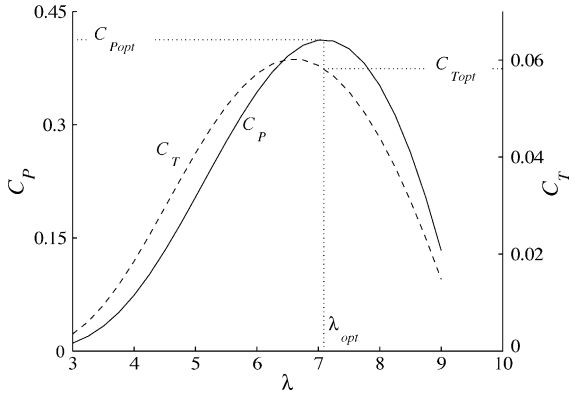

Fig. 2. Torque (dashed) and power (solid) coefficients of the turbine.

$I_H - V_H$ characteristic is influenced by the electrolyte temperature T and can be approximated by a logarithmic law [13]:

$$V_H = V_r + n(T)I_H + m(T)\lg\left(1 + \frac{q(T)}{T^2}I_H\right) \quad (6)$$

where V_r is the reversible cell voltage and $n(T)$, $m(T)$ and $q(T)$ are quadratic functions of T. Fig. 4 plots the $I_H - V_H$ curves of a 2.25 kW von Hoerner electrolyzer for two limit temperatures [14].

2.2. The controller

Stand-alone hydrogen production systems need several control loops as well as a supervisory control. In this paper, we focus on the control of the subsystem comprising the wind turbine, the generator, the ac–dc converter and the electrolyzer. In fact, this subsystem requires a special treatment because it is the most affected by wind resource variability. The main control objective is the maximization of the energy captured by the turbine satisfying at the same time the following requirements for proper operation of the electrolyzer [15]:

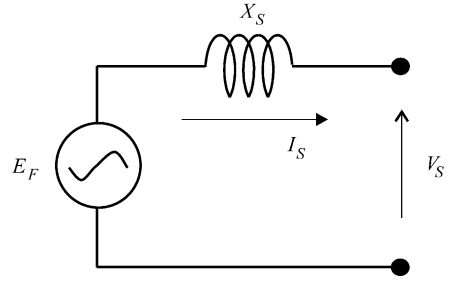

Fig. 3. Per-phase model of the permanent magnet synchronous generator.

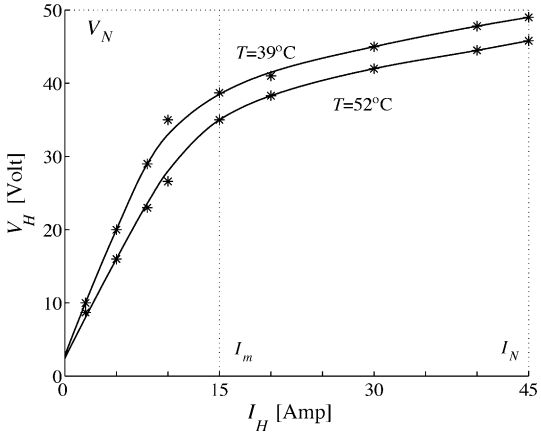

Fig. 4. Current–voltage characteristic of the electrolyzer.

(1) Current and voltage must be upper-bounded at their rated values, I_N and V_N, respectively. In fact, though operation at high current levels is desired to improve the efficiency of the electrolyzer, the system must be maintained within its safe operation area.
(2) A minimum current I_m must be guaranteed with minimal connection to the auxiliary power supply because operation at low currents affects the quality of the product.
(3) The wind power must be smoothed before being supplied to the electrolyzer. As reported in some recent studies, variability of the electrolyzer power may increase the internal wear as well as the impurities and energy losses. So, limiting the rate of change of the input power is desired.

Note: Although these items are established to suitably supply an electrolyzer with wind power, similar specifications could be additionally stated for the battery pack. Moreover, though the proposed control strategy is particulary focused on wind-powered electrolyzers, it is also applicable to other renewable-electrolysis systems.

Fig. 5 shows a schematic diagram of the control system proposed in this paper. It basically consists of an MPPT controller conventionally used in wind turbine control and a novel power reference conditioning loop proposed here to accomplish the specifications of the electrolyzer. The proposed conditioning circuit is enclosed with dashed line in Fig. 5.

Let ignore for the moment the conditioning circuit and focus on the MPPT. That is, let suppose that $P_R = P^*$. The MPPT comprises an outer control loop and an inner control loop. The former computes the optimum power reference as function of the shaft speed, assuming that the turbine is

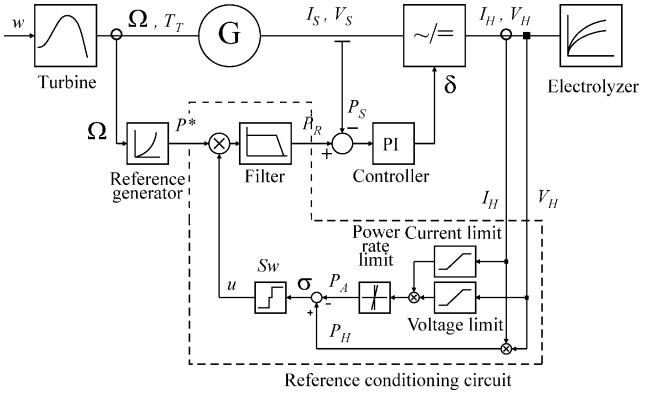

Fig. 5. Scheme of the control system with the proposed reference conditioning.

operating at the optimum tip-speed-ratio:

$$P^*(\Omega) = P_{\text{opt}}(r\Omega/\lambda_{\text{opt}}) = \frac{1}{2}\rho\pi r^5 \frac{C_{\text{Popt}}}{\lambda_{\text{opt}}^3}\Omega^3. \tag{7}$$

The latter, i.e. the inner loop, adjusts the duty cycle of the electronic converter in order to track the reference power P_{R}. In this loop, a conventional PI controller is usually employed to cancel steady state errors. As a result, the turbine speed Ω converges to the optimum value $\Omega_{\text{opt}}(w) = \lambda_{\text{opt}} w/r$. Hence, the maximum power point $(\Omega_{\text{opt}}(w),\ P_{\text{opt}}(w))$ is successfully tracked with the closed-loop dynamic response dominated by the drive-train.

MPPT control, with its inherent variable-speed operation, has an additional advantage with respect to fixed-speed operation. In fact, the more flexible connection to the electric grid provides damping at the resonance modes of the drive-train, thus reducing high frequency oscillations of torque and power. Despite this power quality improvement, MPPT control strategies usually violate the particular specifications of the electrolyzer. In fact, the captured power may exceed the rated power of the electrolyzer and must be limited. Additionally, the torque efforts developed to track the optimum power point translate into fast changes of the electric power that are transmitted to the electrolyzer through the fast electronic devices. This is not an easy problem to solve. On one hand, smoothing the power reference $P^*(\Omega)$ via a low-pass filter may lead to undesirable transient responses. Moreover, the turbine may slow to a stop when the wind velocity drops. On the other hand, slowing down the response of the inner loop may make the overall system unstable too. Then, a feasible option to overcome this problem would be the design of an MPPT controller taking the electrolyzer specifications into account from the beginning. This is a difficult task because of the nonlinear behavior of all the devices involved in the system.

In this paper, a completely different approach is explored. In fact, ideas of power tracking control are still used, but now, an auxiliary reference conditioning loop is incorporated. The aim of this loop is shaping the power reference in order to limit the rate of change of the input power as well as the voltage and current magnitudes. Hence, the captured energy is increased while the requirements of the electrolyzer are satisfied. Reference conditioning is carried out in a controlled fashion, thus preserving stability. This proposal for the control of the wind-powered electrolyzer is the main contribution of the paper and is described in more detail in the following section.

3. Electrolyzer power conditioning control strategy

In this section, a control algorithm to satisfy the additional specifications enumerated above for the electrolyzer is presented. It consists in shaping the power reference via a discontinuous control action using tools of sliding mode control (SMC) theory. Reference conditioning using SMC concepts was originally proposed to design anti-windup techniques for constrained process control [16]. In this case, similar ideas are used to limit the operating ranges of the electrolyzer.

3.1. Background on sliding mode control

A variable structure system comprises a set of continuous subsystems with an associated switching function that determines a manifold on the state space, the so-called sliding surface. According to the sign of the switching function, the control signal takes one of different possible values, leading to a discontinuous control law. The basic idea is to enforce the state to reach the prescribed sliding surface and, henceforth, to slide on it through a very fast switching action. Once this particular mode of operation is established, known as sliding mode (SM) or sliding regime, the prescribed manifold imposes the new system dynamics. Among other attractive features, sliding regimes are easy to implement, reduce the order of the system dynamics, and provide robustness to matched uncertainties and external disturbances [17–19].

Consider the following dynamical system:

$$\frac{\mathrm{d}x}{\mathrm{d}t} = f(x) + g(x)u \tag{8}$$

where $x \in \Re^n$ is the system state, u the discontinuous control signal, and $f(x)$ and $g(x)$ are vector fields in $\Re^n$. The variable structure control law is defined as:

$$u = \begin{cases} u^-, & \text{if } \sigma(x) < 0 \\ u^+, & \text{if } \sigma(x) > 0 \end{cases} \tag{9}$$

according to the sign of the auxiliary output $\sigma(x)$. The sliding surface $\mathcal{S}$ is defined as the manifold, where the auxiliary output, also called switching function, vanishes. That is,

$$\mathcal{S} = \{x \in \Re^n \,|\, \sigma(x) = 0\}. \tag{10}$$

When, as a result of the switching policy (9), the reaching condition:

$$\lim_{\sigma \to 0} \sigma\dot{\sigma} < 0 \tag{11}$$

locally holds at both sides of the surface, a switching sequence at very high frequency (ideally infinite) occurs, constraining the system state trajectory to slide on $\mathcal{S}$.

For a sliding motion to exist on $\mathcal{S}$ (in other words, to satisfy condition (11)), the auxiliary output $\sigma(x)$ must have unitary relative degree, i.e. its first derivative must explicitly depend on u. Additionally, the signals u^+ and u^- must be selected properly.

Note: In the case of linear systems, the relative degree is given by the difference between the numbers of poles and zeros of the transfer function.

3.2. Proposed conditioning technique

3.2.1. The admissible power

The specifications of the electrolyzer regarding voltage limit, current limits and power rate limits translate into lower and upper power limit signals $\overline{P_A}(t)$ and $\underline{P_A}(t)$. On the one hand, the upper limit signal $\overline{P_A}(t)$ is determined by either of the rated values I_N or V_N, or the upper power rate limit. On the other hand, the lower limit signal $\underline{P_A}(t)$ is established by I_m or the lower power rate limit. It is defined here the admissible power $P_A(t)$, which is constructed by passing the electrolyzer current through a limiter upper-bounded at the rated current I_N and lower-bounded at the minimum current I_m, the voltage through a limiter upper-bounded at the rated value V_N and their product through a rate limiter. By construction, this admissible power ranges over $\underline{P_A}(t) \leq P_A(t) \leq \overline{P_A}(t)$ at any time t. So, the specifications for the electrolyzer will be effectively satisfied whenever the actual electrolyzer power equals this admissible power ($P_H(t) = P_A(t)$).

On the basis of this analysis, the following output signal is defined:

$$\sigma = P_H - P_A(t). \tag{12}$$

Note that whereas (10) defines a surface in conventional sliding mode control, in the current application $\sigma \equiv 0$ determines a region in the state space, where P_H is constrained within its admissible limit values $\underline{P_A}(t)$ and $\overline{P_A}(t)$. In fact, this region defined by $\mathcal{R} = \{\sigma = P_H - P_A(t) = 0\}$ is delimited by two time-varying surfaces $\overline{\mathcal{S}}$ and $\underline{\mathcal{S}}$ defined by $\overline{\mathcal{S}} = \{\overline{\sigma} = P_H - \overline{P_A}(t) = 0\}$ and $\underline{\mathcal{S}} = \{\underline{\sigma} = P_H - \underline{P_A}(t) = 0\}$, respectively.

3.2.2. The SM conditioning objective

Obviously, the specifications of the electrolyzer are satisfied whenever the auxiliary output (12) is set to zero. Thus, the objective of the conditioning loop is to maintain the system operating in the desired region $\mathcal{R}$, i.e. to constrain P_H between its limit values $\overline{P_A}(t)$ and $\underline{P_A}(t)$ all the time. So, when P_H tries to cross any of the associated limit surfaces, $\overline{\mathcal{S}}$ or $\underline{\mathcal{S}}$, a sliding regime is established until P_H is able to evolve toward the interior of $\mathcal{R}$ without correction.

In contrast with conventional SMC, the aim of the control strategy proposed here is not to evolve in sliding mode towards the equilibrium point. Contrarily, the sliding regime is intended as a transitional mode of operation. It is aimed at conditioning the power reference in order to accomplish the specifications of the electrolyzer. Hence, once the captured power evolves smoothly and within the permissible limits, the sliding mode correction becomes inactive.

3.2.3. The conditioning loop

The conditioning system within dashed lines in Fig. 5 comprises a block devoted to compute the admissible power P_A as detailed above, a comparator that determines the auxiliary output σ, a switching logic that decides the control signal u and a first-order low-pass filter F interposed in the path of the power reference signal. Note that, from the point of view of implementation, this conditioning system can be realized as a set of instructions at the software level of the MPPT controller. So, the only additional hardware is the on-line measurement of the electrical variables of the electrolyzer.

The MPPT reference $P^*(\Omega)$ is affected by the discontinuous factor u before passing through the low-pass filter. It must be remarked that this filter is not intended to smooth by itself the reference. In fact, this obvious approach could lead to instability as explained before. Conversely, the proposed conditioning lies in shaping the filter output P_R as function of the electrolyzer specifications. So, the cut-off frequency of the filter is designed to attenuate the switching frequency but fast enough to avoid introducing appreciable lags. The power reference P_R is thus a smooth signal shaped by the SM control loop through the discontinuous input signal u.

3.2.4. The switching logic

Before proposing a switching law, it will be checked the relative degree of the output σ with respect to the discontinuous control signal u. Note that σ and u are the output and input, respectively, of a cascade system comprising the filter F, the PI controller and the ac–dc converter. The filter and PI controller are linear dynamical systems described by the transfer functions

$$\begin{aligned} &\mathrm{F}: F(s) = \frac{1}{1 + s\tau_F} \\ &\mathrm{PI}: C(s) = K_P\left(1 + \frac{1}{s\tau_C}\right) \end{aligned} \tag{13}$$

where τ_F is the time constant of the filter, K_P the proportional gain, τ_C the integral time of the controller and s is the Laplace operator. Finally, the ac–dc converter may be described by the static input–output Eq. (5). Whereas the filter F has unitary relative degree (it has one pole and no zero), the PI controller (one pole and one zero) and the converter (its outputs V_H and I_H explicitly depend on its input δ) have null relative degree. So, the cascade system F–PI– $\sim$ / = effectively has unitary relative degree. This means that the necessary condition for SM existence on surfaces $\overline{\mathcal{S}}$ and $\underline{\mathcal{S}}$ is satisfied. Then, sliding regimes on the borders of the desired operating region $\mathcal{R}$ can be established provided an adequate switching logic is

decided [16]. We propose here:

$$Sw: \begin{cases} u^- = 1, & \text{if } \sigma < 0 \\ u^0 = k, & \text{if } \sigma = 0 \\ u^+ = 0, & \text{if } \sigma > 0 \end{cases} \quad (14)$$

Naturally, the sustainable limits for the conditioning action are optimum power ($u \equiv 1$) and no power ($u \equiv 0$). The signals u^- and u^+ are designed in consequence. Finally, $u^0 = k < 1$ is designed as a compromise between efficiency and available control effort. In fact, with regards to energy production, the parameter k should be selected close to 1 so that $P_R \approx P^*(\Omega)$ during desired operation mode ($\sigma \equiv 0$). Nevertheless a factor k close to 1 would minimize the capability of conditioning the electrolyzer power during sudden wind speed decrease. It must be remarked that this type of compromise commonly appears in control of wind energy systems when the quality of the power supplied to the grid or load is an important issue. In our application, sacrificing some percent of the wind energy may be largely rewarded by the improvement of the electrolyzer power quality as well as of the produced hydrogen one. Actually, since the turbine is often oversized to avoid multiple connections and disconnections of the electrolyzer to the turbine, some reduction of the captured energy is not a serious disadvantage. Moreover, the available wind power may well exceed the rated power of the electrolyzer during long periods and the power capture should be deliberately further reduced for safety operation of the electrolyzer.

3.2.5. SM conditioning loop operation

The conditioning system operates as follows. Let suppose that, initially, the input power to the electrolyzer satisfies the specifications and, therefore, $u = u^0 = k$. Let suppose now that the wind speed (and consequently the reference power P_R) increases in such a way that the rated values of current/voltage at electrolyzer terminals, or its power rate upper limit is reached at time t. At that moment, the actual electrolyzer power $P_H(t)$ reaches its maximum permissible value $\overline{P_A}(t)$. Immediately after $P_H(t)$ tries to exceed $\overline{P_A}(t)$, u switches to $u^+ = 0$, thus reducing the reference power. When this occurs, u returns to its default value $u^0 = k$, so P_H will try to exceed $\overline{P_A}(t)$ again. Consequently, a series of high frequency commutations between $u = k$ and $u = 0$ takes place, establishing a sliding mode on $\overline{\mathcal{S}}$ until the limitations become inactive ($P_H \equiv P_A(t)$ with $u = u^0$). That is, when P_H evolves to the interior of the desired operating region. This occurs when the voltage, current and power rate fall below their rated values after the wind speed slows down.

Conversely, when P_H tries to fall below $\underline{P_A}$ (that is, when the minimum current is reached or the captured power drops suddenly because of a decreasing wind gust), the factor u switches to $u^- = 1$. In fact, the controller tries to increase the supplied power in order to restore immediately the desired operating mode. When this is achieved, u switches again to $u^0 = k$. As a result, a sliding regime is established on $\underline{\mathcal{S}}$, with u switching between $u = k$ and $u = 1$. When the limitation disappears because a favorable change in the wind conditions, the normal operation ($u = k$) is recovered and the electrolyzer variables evolve to the interior of their permissible ranges of variation without sliding mode conditioning.

Note that, independently of the control strategy, the control effort that is available to attenuate the effects of wind drops in wind energy systems is limited. In fact, the energy stored in the rotor that can be used to supply the power shortage is bounded. In the current application, the bounded control action means that the sliding mode conditioning cannot be sustained under drastic wind reductions. In fact, if the wind decreases too fast, the energy stored in the rotor may not be sufficient to maintain P_H above its lower power rate limit and u will be fixed at $u^- = 1$ trying to provide as much energy as possible to the electrolyzer during the transient. Similarly, if the wind decreases to a too small value, the available wind power will inevitably be not sufficient to supply the current I_m to the electrolyzer. This limitation is not attributable to the control strategy but to the resource availability. In fact, if the input power required to supply the current I_m to the electrolyzer exceeds the available in the wind ($P_{opt}(w)$), maintaining the minimum electrolyzer current will not be achievable, independently of the control strategy. In this case, the backup power supply should be connected.

4. Simulation results

In this section, simulation results are presented. They were obtained for a system like that shown in Fig. 1 with a 2.25 kW electrolyzer and a 5 kW wind turbine plus permanent magnet induction generator. For the sake of clarity in the presentation of the simulation results, the electrolyte temperature T was considered constant. Under this assumption, current and voltage bounds lead to constant power limit signals.

The wind speed used in simulations is plotted in Fig. 6. This wind profile has been intentionally selected to evaluate the performance of the control strategy under extreme conditions. The results of three simulation runs are presented. The first two sets of data (cases A and B) were obtained without the conditioning loop, whereas sliding mode conditioning is included in the last simulation run (case C).

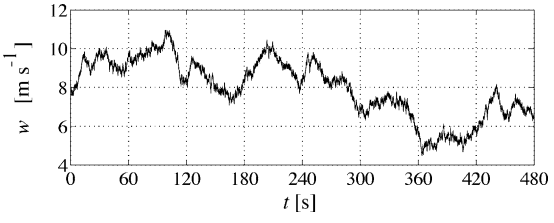

Fig. 6. Wind speed profile.

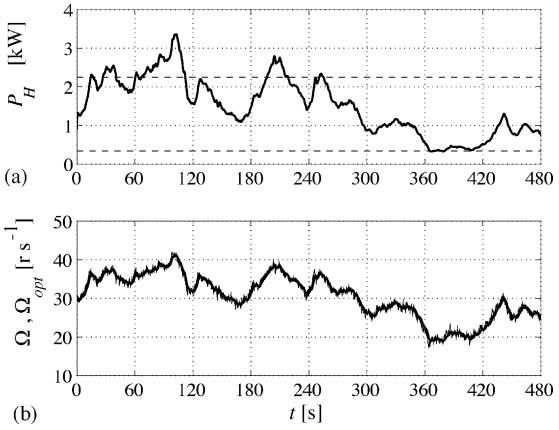

Fig. 7. Simulation results with MPPT: (a) electrolyzer power and (b) actual (thick trace) and optimum (noisy trace, overlapped) turbine speed.

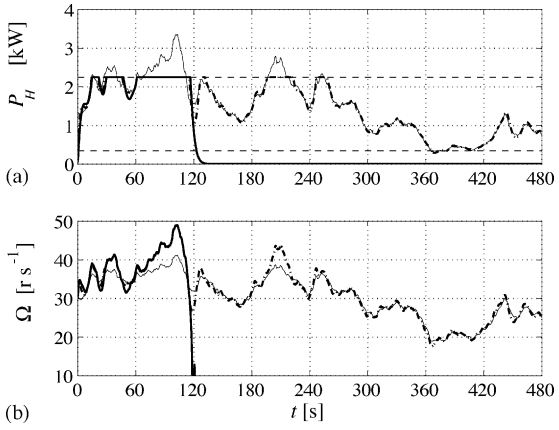

Fig. 8. Simulation results with filtered reference (dot-dashed: $\tau_C = 2$ s, solid: $\tau_C = 3$ s, thin: without filter): (a) electrolyzer power and (b) turbine speed.

4.1. Case A: maximum power tracking control

This case is devoted to show the performance of the conventional MPPT algorithm for comparison with the proposed control (case C). The results are presented in Fig. 7. Fig. 7a depicts the power captured by the turbine and supplied to the electrolyzer. Fig. 7b displays the optimum speed profile overlapped by the actual turbine speed. In fact, the optimum speed (for maximum power capture) is successfully tracked with the mechanical dynamics that is too fast to be distinguished in the time scale of the figure. Thus, the electrolyzer power also overlaps the optimum turbine power $P_{opt}(w)$. Note that, although the optimum operating point of the turbine is successfully tracked, the MPPT performance does not accomplish the power requirements of the electrolyzer. In fact, the supplied power reproduces the fast wind variations and exceeds during some time intervals its rated value as well as its power rate limit.

The option of smoothing the power reference $P^*(\Omega)$ with a low-pass filter is evaluated here. Reference filtering is often used in many control problems to avoid nonlinearities or undesirable responses. However, this approach does not provide a satisfactory solution in this application. Fig. 8 shows the simulation results obtained when the power reference $P^*(\Omega)$ is passed through a first-order filter to smooth fluctuations and then limited at rated power. Results are presented for two cases: $\tau_{C1} = 2$ s and $\tau_{C1} = 3$ s, with τ_C being the time constant of the filter. In neither of the two cases, the filter smoothes substantially the power fluctuations. Moreover, in the latter case, where the cut-off frequency is lower, the filter introduces a lag that leads to a turbine stop. This undesirable behavior has been predicted in Section 2.2. Because of the filter lag, the filtered reference often exceeds the captured power when wind drops, hence decelerating the rotor below the optimum speed. In particular, the wind gust at $t = 120$ s drives the turbine into the stall region (see in Fig. 8b that the rotor speed falls well below the optimum speed, i.e. $\lambda \ll \lambda_{opt}$), where the system presents an unstable behavior. Since wind varies randomly, there is no guarantee of stability when a low-pass filter is used to smooth the reference power.

4.2. Case B: suboptimum power point tracking

This control strategy is a prelude of the SM conditioning technique evaluated in the following paragraph. It basically consists of the conventional MPPT algorithm, where the reference power locus is obtained by multiplying $P^*(\Omega)$ by a coefficient $k < 1$, more precisely $k = 0.7$. That is, $P_R = 0.7P^*(\Omega)$. Note that this selection of k does not imply a 30% reduction of the captured power with respect to the optimum case. In reality, the system searches a new operating point q_k at higher speeds, where the power reference curve $kP^*(\Omega)$ crosses the actual power-speed locus of the turbine (see Fig. 9). At this new point, the turbine operates with a power coefficient, lower than C_{Popt} of course, that depends on the shape of its C_P–λ curve.

Fig. 10 shows the simulation results. Fig. 10a illustrates the captured power which also violates the specifications of the electrolyzer. In fact, during the simulation run, the supplied power exceeds its rated value (2.25 kW), falls below its

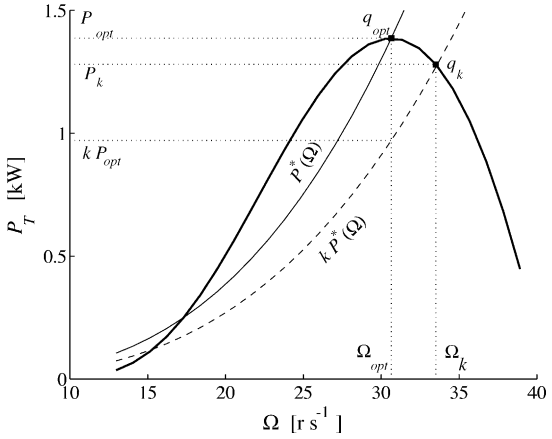

Fig. 9. Operating points for different power reference loci.

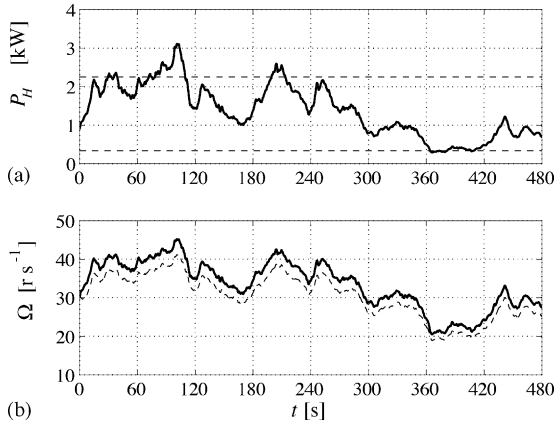

Fig. 10. Simulation results with suboptimum power tracking: (a) electrolyzer power and (b) turbine speed (solid line) and turbine speed for case A (dashed line).

minimum permissible value (0.35 kW in this example) and presents fast variations. Fig. 10b reveals that the turbine is effectively operating at a speed higher than in case A, thereby reducing the energy capture as expected. Actually, after comparing the captured power in this case and in the previous optimum case, it follows that the energy loss is around 7%.

4.3. Case C: suboptimum power point tracking with sliding mode conditioning to satisfy the electrolyzer power requirements

The simulation results obtained with the proposed control algorithm are shown in Fig. 11. In Fig. 11a, the power supplied to the electrolyzer P_H, which tightly follows the conditioned reference P_R, is plotted. Fig. 11b exhibits the turbine speed response. Fig. 11c displays the discontinuous conditioning signal. Finally, Fig. 11d depicts the auxiliary output response.

The simulation results corroborate the effectiveness of the proposed conditioning. In fact, the electrolyzer current has been bounded below its rated value and the captured power has been smoothed, thereby improving the quality of the power supplied to the electrolyzer.

As clearly observed in Fig. 11c, the simulation run alternates intervals of SM conditioning with periods of no correction. In fact, the SM conditioning periods are identified by the fast switching behavior of the discontinuous signal u. Moreover, sliding regimes occur on the upper-limit surface $\overline{\sigma} = 0$ when u switches between u^0 and 0, whereas they are established on the lower-limit surface $\underline{\sigma} = 0$ when u switches between u^0 and 1. On the other hand, the conditioning loop is inactive during the nonzero time intervals, where u is fixed at u^0.

Fig. 11a shows how the conditioning loop shapes the electrolyzer power with the aim of accomplishing the specifications. For instance, from $t = 0$ to 34 s, the sliding regime is able to constrain P_H to its maximum permissible rate of change despite the rapidly increasing wind power. Similarly, the sliding regime between $t = 40$ and 54 s limits the decreasing rate of change to its lowest admissible value. Also, the SM conditioning between $t = 78$ and 114 s successfully confines I_H (and hence P_H) to its rated value. Finally, from $t = 365$ to 382 s, the sliding mode increases the reference power, thus avoiding I_H to fall below I_m. Besides, during other periods, the electrolyzer power evolves smoothly and within its permissible values without SM conditioning. See, for instance, the response from $t = 382$ to 430 s.

Fig. 11b illustrates how the turbine adjusts its speed in order to supply an appropriate amount of power to the electrolyzer. Note that the speed is above the optimum turbine speed most of the time, particularly during regulation at rated power or maximum power rate, whereas it approaches Ω_{opt} during regulation at minimum power or minimum power rate.

Fig. 11d confirms that P_H is maintained within the desired region of operation ($\sigma \equiv 0$) all the time except for a short period around $t = 120$ s. During this period, characterized by a fast decreasing gust, the conditioning loop applies the maximum control effort to increase as much as possible the captured power. Thus, during this period the controller behaves as an MPPT control. This kind of behavior is not completely avoidable because the available control effort is limited. The compromise in the design of k between energy capture and

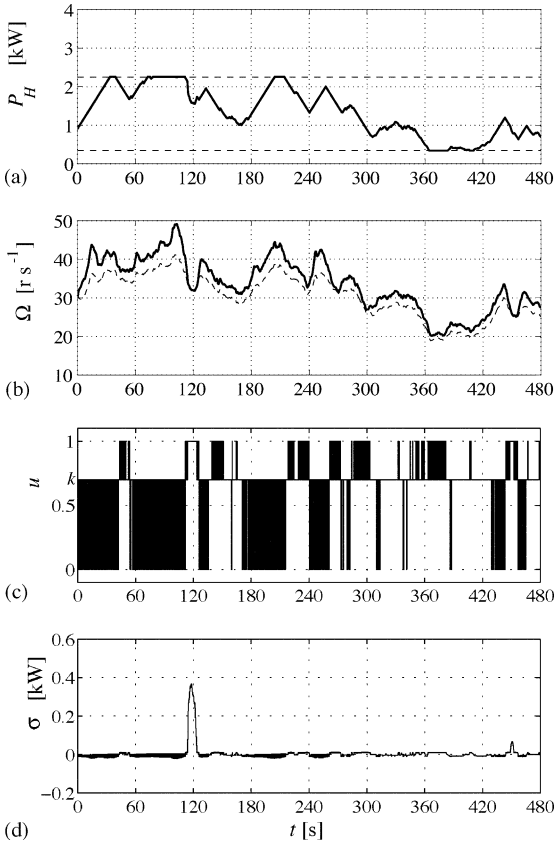

Fig. 11. Simulation results with suboptimum power tracking and SM conditioning: (a) electrolyzer power; (b) turbine speed (solid line) and turbine speed for case A (dashed line); (c) SM control signal; (d) SM auxiliary output.

power quality improvement is evident. Although the sliding regime cannot be sustained during this short period, the overall response is much better than in the unconditioned case.

5. Conclusions

The power control of a wind–hydrogenenergy system has been addressed. The proposed controller basically combines a maximum power point tracking algorithm (such those conventionally used to maximize efficiency in wind energy systems) and a novel auxiliary loop that suits the captured power to the requirements of the electrolyzer. Actually, this loop shapes the power reference, when necessary, guaranteing safe operation of the electrolyzer and improving the conditions for hydrogen production. The reference conditioning circuit is designed using concepts of sliding mode control theory. The proposed solution is very simple to implement and tune, and shows a very fast response. Furthermore, it can be readily incorporated to pre-existing maximum power point tracking controllers. The ability of the controller to shape properly the power profile has been corroborated by a simulation example.

Acknowledgements

This work was partially funded by ANPCyT (PICT2003 11-14111), CICpBA (Grant Res. 694/04), CONICET (Grant Res. 691/04) and UNLP.

References

[1] R. Dell, D. Rand, Energy storage: a key technology for global energy sustainability, J. Power Sources 100 (1) (2001) 2–17.
[2] B. Shakya, L. Aye, P. Musgrave, Technical feasibility and financial analysis of hybrid wind–photovoltaic system with hydrogen production for cooma, Int. J. Hydrogen Energy 30 (1) (2005) 9–20.
[3] S. Vosen, J. Keller, Hybrid energy storage systems for stand-alone electric power systems: optimization of system performance and cost through control strategies, Int. J. Hydrogen Energy 24 (12) (1999) 1139–1156.
[4] G. Crabtree, M. Dresselhaus, M. Buchanan, The hydrogen economy, Science 305 (5686) (2004) 958–974.
[5] K. Agbossou, R. Chahine, J. Hamelin, F. Laurencelle, A. Anouar, Renewable energy systems based on hydrogen for remote applications, J. Power Sources 96 (1) (2001) 168–172.
[6] K. Agbossou, M. Kolhe, J. Hamelin, T. Kose, Performance of a stand-alone renewable energy system based on energy storage as hydrogen, IEEE Trans. Energy Convers. 19 (3) (2004) 633–640.
[7] M. Eskander, T. El-Shatter, M. El-Hangry, Energy flow and management of a hybrid wind/pv/fuel cell generation system, in: IEEE 33rd Annual Power Electronics Specialists Conference (PESC), vol. 1, 2002, pp. 347–353.
[8] L. Grimsmo, M. Korpaas, T. Gjengedal, S. Moller-Holst, A study of a stand alone wind and hydrogen system, in: Nordic Wind Power Conference, Chalmers, 2004, pp. 1–6.
[9] L. Fingersh, Optimized hydrogen and electricity generation from wind, Technical Report TP-500–34364, NREL, CO, June 2003.
[10] C. Elam, B. Kroposki, G. Bianchi, K. Harrison, Renewable electrolysis integrated system development and testing, Progress Report FY2004, DOE Hydrogen Program, NREL, CO, 2004.
[11] L. Freris (Ed.), Wind Energy Conversion Systems, Prentice Hall, Hertfordshire, UK, 1990.
[12] N. Mohan, T. Undeland, W. Robbins, Power Electronics: Converters, Applications and Design, third ed., John Wiley & sons, NY, 2003.
[13] Ø. Ulleberg, Modeling of advanced alkaline electrolyzers: a system simulation approach, Int. J. Hydrogen Energy 28 (1) (2003) 21–33.
[14] T. Schucan, Case studies of integrated hydrogen energy systems, International Energy Agency Hydrogen Implementing Agreement, Final Report, Paul Scherrer Institute, Switzerland, 2000.
[15] A. Dutton, J. Bleijs, H. Dienhart, M. Falchetta, W. Hug, D. Prischich, A. Ruddell, Experience in the design, sizing, economics, and implementation of autonomous wind-powered hydrogen production systems, Int. J. Hydrogen Energy 25 (8) (2000) 705–722.
[16] R. Mantz, H. De Battista, Sliding mode compensation for windup and direction of control problems in two-input–two-output PI controllers, Ind. Eng. Chem. Res. 41 (2002) 3179–3185.
[17] H. Sira-Ramírez, Differential geometric methods in variable structure systems, Int. J. Control 48 (4) (1988) 1359–1390.
[18] J. Hung, W. Gao, J. Hung, Variable structure control: a survey, IEEE Trans. Ind. Electron. 40 (1) (1993) 2–22.
[19] V. Utkin, J. Guldner, J. Shi, Sliding Mode Control in Electromechanical Systems, first ed., Taylor & Francis, London, 1999.